Shustikova, I., Domeneghetti, A., Neal, J. C., Bates, P., & Castellarin, A. (2019). Comparing 2D capabilities of HEC-RAS and LISFLOOD-FP on complex topography. *Hydrological Sciences Journal*, *64*(14), 1769-1782. https://doi.org/10.1080/02626667.2019.1671982

Comparing 2D capabilities of HEC-RAS and LISFLOOD-FP on complex topography.

Journal:	*Hydrological Sciences Journal*
Manuscript ID	HSJ-2019-0168.R1
Manuscript Type:	Original Article
Date Submitted by the Author:	04-Jul-2019
Complete List of Authors:	Shustikova, Iuliia; University of Bologna, Department of Civil, Chemical, Environmental, and Materials Engineering - DICAM Domeneghetti, Alessio; University of Bologna, Department of Civil, Chemical, Environmental and Materials Engineering - (DICAM) Neal, Jeffrey; University of Bristol, School of Geographical Sciences Bates, Paul; University of Bristol, School of Geographical Sciences Castellarin, Attilio; University of Bologna, Department of Civil, Chemical, Environmental and Materials Engineering - (DICAM)
Keywords:	hydraulic modelling, two-dimensional models, floodplain inundation, DEM resolution

Comparing 2D capabilities of HEC-RAS and LISFLOOD-FP on complex topography.

Iuliia Shustikova[a], Alessio Domeneghetti[a], Jeffrey C. Neal[b], Paul Bates[b], Attilio Castellarin[a]

[a]*Department of Civil, Chemical, Environmental and Materials Engineering (DICAM), School of Civil Engineering, University of Bologna, Bologna, Italy (iuliia.shustikova@unibo.it),*

[b]*School of Geographical Sciences, University of Bristol, Clifton, Bristol, BS8 1SS. UK*

Abstract: This study evaluates and compares two-dimensional (2D) numerical models of different complexity by testing them on a floodplain inundation event that occurred on the Secchia River (Italy). We test 2D capabilities of LISFLOOD-FP and HEC-RAS (5.0.3); implemented using various grid size (25-100m) based on 1m DEM resolution. As expected, best results were shown by the higher resolution grids of 25m for both models, which is justified by the complex terrain of the area. However, the coarser resolution simulations (50 and 100m) performed virtually identical compared to high-resolution simulations. Nevertheless, spatial distribution of flood characteristics varies; the 50 and 100m results of LISFLOOD-FP and HEC-RAS misestimated flood extent and water depth in selected control areas (built-up zones). We suggest that the specific terrain of the area can cause ambiguities in large-scale modelling, while providing plausible results in terms of the overall performance.

Keywords: Floodplain inundation, hydraulic modelling, two-dimensional models, DEM resolution

1. Introduction

Recent and historical data demonstrate the large share of monetary damage and fatalities that can be attributed to hydrological natural hazards (Munich RE 2015b). Some of the most costly floods in the past decades occurred in central European countries, for example the 2002 flood resulted in 16.5 billion $ and 2013 about 12.5 billion $ damage, altogether caused 64 deaths (Munich RE 2015a). Additionally, a related issue is climate change, which will likely to affect the frequency and magnitude of floods in the future (Milly et al. 2002; Lehner et al. 2006; Alfieri et al. 2015; Arnell and Gosling 2016). With global economic and population growth the consequences of severe flooding events induced by climate change are likely to increase in the future, so the overall flood risk is projected to increase significantly (Alfieri et al. 2017). Although some studies demonstrate the difficulty of predicting future flood frequency and magnitude changes due to the high complexity of forcing mechanisms, it is evident that the flood damages will continue to grow (Kundzewicz et al. 2013). Such conditions emphasise the importance of developing efficient flood risk management strategies which would help to lower the upcoming losses. The 2007 European Flood Directive (2007/60/EC), among others, contributes to increasing resilience to hydrological natural disasters by requiring each EU Member State to develop cyclically updated flood hazard and risk maps and establishing long-term management plans (EC 2007).

The Flood Directive identifies flood risk as “a product of the probability of the flood event and its potential adverse consequences” (EC 2007), and it has to be re-assessed and updated every six years. Therefore, a crucial element in flood risk assessment is efficient and accurate flood hazard mapping and, functional to this, the identification of the most suitable models and tools for adequately addressing this task, thereby enhancing the overall quality of risk analysis.

A considerable number of studies have demonstrated the use of the one- and two-dimensional (1D and 2D) numerical models to delineate floodplains (Bates and Roo 2000; Aronica et al. 2002; Horritt and Bates 2002; Büchele et al. 2006; Moel et al. 2009; Di Baldassare et al. 2009; Neal et al. 2012; Falter et al. 2013; Domeneghetti et al. 2013; Alfieri et al. 2014; Domeneghetti et al. 2015; Di Baldassare et al. 2010), which allow an accurate representation of river hydraulics and floodplain inundation dynamics. There is an ongoing debate, however, on which schematization under which conditions should be used (1D, coupled 1-2D or fully 2D) (Apel et al. 2009).

Recent studies suggest using fully 2D models with high level of details in order to avoid uncertainties and limitations coming from the incorrect interpretation of flood dynamics and

unrealistic reproductions of the terrain topography (Morsy et al. 2018). Some studies, however, point out that for the large scale studies, coarser resolution (i.e. 50m) is an optimum between the accuracy and computational expenses for 2D simulations (Savage et al. 2016). While 1D models have proved to be able to represent the processes within the channel, the flood wave dynamics across inundated floodplains can be only captured using 2D scheme (Tayefi et al. 2007; Falter et al. 2013). Using fully 2D codes can, however, be difficult, as most areas are not covered by the high-resolution terrain datasets (LiDAR surveys) that such modelling requires. In addition, another evident constraint of using fully 2D codes lies in their higher computational burden relative to simplified coupled 1D/2D codes (Apel et al. 2009; Falter et al. 2013; Dimitriadis et al. 2016). Yet, the tendency to run high-resolution global and regional flood scenarios is increasing (Falter et al. 2013; Sampson et al. 2015; Savage et al. 2016; Schumann et al. 2016, 2016). Furthermore, with increasing computational capacity, parallelization techniques and affordable access to cloud computing services, the utilisation of 2D codes in combination with high-resolution DEMs becomes more and more viable for hydraulic engineers and researchers (Morsy et al. 2018). Moreover, the 20x and 100x speed-ups gained by executing codes on graphical processing units (GPU) hardware comparing to central processing unit (CPU) clusters show the potential in applying high-resolution flood models over large areas (Vacondio et al. 2014; Morsy et al. 2018).

Among 2D models, there are codes, which use fully 2D shallow-water or diffusion wave equations and those, which simplify certain terms (Teng et al. 2017). The main differences in the performance of such models lie in the governing equations used, the mesh representation (structured, unstructured, raster-based, flexible) and numerical scheme (finite-element, finite-volume, finite-difference). Simplified 2D models have a solid advantage by being computationally significantly more efficient than, for instance, fully 2D models based on the complete Saint-Venant equation (Néelz S. and Pender G. 2013). Previous research done in this domain has covered benchmark analysis of a number of 2D codes. A benchmark study performed by the UK Environment Agency on 2D hydraulic modelling packages revealed that 2D models based on shallow-water equations deliver better results in terms of flood water velocity, than the ones which used simplified equations (Néelz S. and Pender G. 2013). Nevertheless, the same study clearly indicates that for the representation of flood extent all 2D packages perform comparably (those which solve full shallow water equations and those, which neglect/simplify certain terms). Another benchmarking study for 2D codes was performed by Hunter et al. (2008) who compared six 2D codes of different complexity for urban flood modelling using hyper-resolution LiDAR data. They concluded that such data is

accurate enough to simulate flow in urban environments, however the uncertainties arise from parameterisation of the models (Hunter et al. 2008). Haile and Rientjes (2005) also investigated 2D flood modelling using LiDAR data and confirmed that urban areas require high-resolution data (maximum 15m grid size) and additional pre-processing to represent buildings. However, such studies are applied solely for urban areas; in different landscapes (natural and artificial) the data resolution and parametrisation should be further investigated.

Building on the existing literature, our study aims at further deepening our knowledge and understanding of the potential and capabilities of different types of 2D inundation models in the context of flood hazard assessment and mapping. In particular, our study compares two models, the well-known LISFLOOD-FP (Horritt and Bates 2002) and the recently launched 2D version (release 5.0.3) of Hydrologic Engineering Center-River Analysis System (HEC-RAS) model. The two codes represent different model complexities, LISFLOOD-FP is a raster-based 2D model based on inertial formulation of the shallow-water equations, while HEC-RAS is a widespread modelling tool for hydraulic engineers that can be used for a large spectrum of applications and deploy different schematization complexities, and, in more recent releases, solves the fully 2D equations.

A previous study performed by Horritt and Bates (2002) looked into differences in terms of flood extent for a 2D diffusion-wave LISFLOOD-FP model, a 1D HEC-RAS model and a 2D finite-element TELEMAC 2D model. They identified that HEC-RAS and TELEMAC 2D are different from LISFLOOD-FP because of their different response to friction coefficients used in calibration (Horritt and Bates 2002). It is important to point out, that this study is based on the older version of the models. For instance, HEC-RAS has been improved and is now used not only for 1D but also for fully 2D simulations with additional advantages of implying fully momentum shallow water equation on high resolution DEMs with unstructured grid., LISFLOOD-FP has also been updated from a diffusion wave to inertial formulation of the shallow water equation and now uses an adaptive time step, which ensures numerical stability of the code.

LISFLOOD-FP and HEC-RAS codes are governed not only by different schemes, but mesh representations, capabilities and input data requirements, and hence a thorough comparison is needed to better understand their advantages and limitations relative to topographical complexity, inundation dynamics and data availability of the codes updated versions. Regional and continental applications of LISFLOOD-FP are already a reality (Alfieri et al. 2014;

Schumann et al. 2016; Sampson et al. 2015), while such applications can be envisaged in the near future for fully 2D HEC-RAS due to the rapid expansion of computational means and strategies cited above. For instance, a recent study by Liu et al. (2019) compared the 1D and 2D modules of HEC-RAS and LISFLOOD-FP where the channel flow is linked to the floodplain by lateral structures using a uniform grid resolution of 30m. They concluded that the 2D models showed slightly better results than 1D. It is crucial to remember, that small and big changes made to the codes together with emerging accuracy of LiDAR data may drastically affect models' performance and results. Therefore, in this study we would focus on the newest versions of the codes and investigate the advantages disadvantages and their correlation with the DEM resolution for floodplain modelling.

Our study aims at quantitatively highlighting differences and similarities in terms of accuracy of representation of inundation processes within heterogeneous floodplains and computational efficiency between the models with regard to different grid and terrain resolutions. We focused our study on such aspects as the capabilities and accuracy of 2D models of different complexity to capture flood extent and water depth in areas with complex topography. Additionally, we discuss model limitations in the context of future large-scale applications of detailed fully 2D models.

2. Tools and study scope

2.1. HEC-RAS (5.0.3)

HEC-RAS (5.0.3) was developed to perform fully 2D computations, and solves both the 2D Saint Venant equations or the 2D Diffusion Wave equations through an implicit finite volume solution. The selection of the equation depends on the study case (dam breach, wave propagation analysis, existence of multiple hydraulic structures within the area) (Brunner 2016). Previous studies done on benchmarking of the codes with different physical complexity showed that, in cases where subcritical flow is unlikely (gradually varied flow), simpler codes perform comparably well in terms of water depth and velocity (Neal et al. 2012; Almeida and Bates 2013). In order to utilise more stable numerical solutions and reduce the computation time for the current case, we selected the 2D Diffusion Wave solver. It identifies the barotropic and bottom friction terms as prevailing.

$$\frac{n^2|V|V}{(R(H))^{4/3}} = -\nabla H \quad (1)$$

The above equation can be further rearranged by dividing both sides by the square root of their norm,

$$V = \frac{-(R(H))^{2/3}}{n} \frac{\nabla H}{|\nabla H|^{1/2}} \quad (2)$$

Where V is the velocity vector, R is the hydraulic radius and $-\nabla H$ is the surface elevation gradient, n is Manning´s n.

The differential form of the Diffusion Wave Approximation of the Shallow Water equation can be obtained by combining the diffusion wave equation in the mass conservation equation,

$$\frac{\partial H}{\partial t} - \nabla \bullet \beta \nabla H + q = 0 \quad (3)$$

Where,

$$\beta = \frac{(R(H))^{5/3}}{n|\nabla H|^{1/2}} \quad (4)$$

(Brunner 2016)

Mesh computation is done automatically within the 2D flow areas and meshes can be structured (i.e. regular connectivity) or unstructured (irregular connectivity). The selection of the grid type (structured/unstructured) depends on the terrain topography and data availability, enabling the user to adopt reduced mesh resolution in more homogenous areas and a highly detailed description along critical terrain features such as embankments or levees. Additionally, the model gives an opportunity to reduce the computation time by implementing a coarser grid on fine topographic details through a so-called sub-grid bathymetry approach (see Figure 1) (Brunner 2016). For instance, the DEM resolution might be 2 meters, while the mesh cell size is 25m (see Figure 1). During a pre-processing step, hydraulic radius, volume and cross-sectional data are collected for each mesh cell using the finer resolution data and stored in property tables (a function for cell face area (A) and water surface elevation (H); see Figure 2). The sub-grid approach allows the computation of more detailed property tables for larger mesh cell sizes.

2.2. LISFLOOD-FP

LISFLOOD-FP is a raster-based low-complexity hydraulic model, which was designed for research purposes and in particular allows for high-resolution simulations. The model used in this paper is employed in 2D mode and solves an inertial formulation of the shallow-water equations in explicit form through a finite difference scheme (Bates et al. 2010; Savage et al. 2016). The model further simplifies the computation by decoupling flows in the x and y

directions and treating the 2D problem as a series of 1D calculations through the cell face boundaries. Therefore, the water flow through each cell face is calculated as:

$$q_{t+\Delta t} = \frac{q_t - g h_t \Delta t \frac{\Delta(h_t+z)}{\Delta x}}{(1+g h_t \Delta t n^2 \, q_t/h_t^{10/3})} \quad (5)$$

Where, $q_{t+\Delta t}$ is a unit flow at the next time step *t*, *g* is gravitational acceleration, *h* is depth, n is a Manning's roughness coefficient, Δ is the cell resolution, *z* is cell elevation, h_t is the difference between highest bed elevation and highest water surface elevation between two cells (Savage et al. 2016; Bates et al. 2010).

The discharge through the four faces of each cell is then used to update the water depth in each cell at each time step:

$$\frac{\Delta h^{i,j}}{\Delta t} = \frac{Q_x^{i-1,j} - Q_x^{i,j} + Q_y^{i,j-1} - Q_y^{i,j}}{\Delta x^2} \quad (6)$$

Where, *i* and *j* are the coordinates of a cell (Coulthard et al. 2013).

In order to secure the model stability we used an adaptive time step based on the Courant-Friedrichs-Lewy (CFL) condition which is estimated as (Bates et al. 2010):

$$\Delta t_{max} = \alpha \frac{\Delta x}{\sqrt{g h_t}} \quad (7)$$

Where α is a coefficient ranging from 0.3 to 0.7, which ensures the numerical stability (Coulthard et al. 2013).

Despite the governing equations used to compute the flow between cells, another important distinction between the two models is the way in which the codes treat topographic data. Differently from HEC-RAS, mesh size in LISFLOOD-FP is forced by the resolution of the input DEM data and cannot be further manipulated. There is not an option to include sub-grid (see details above) terrain in the 2D computations with larger mesh sizes, meaning the mesh face cross-section profile has a rectangular shape.

2.3. Objective of the study

Our study tests and compares the models on an inundation event that occurred on 19th January, 2014 in the dike-protected floodplain of the Secchia River (a right bank tributary of the Po River), Northern Italy (see Figure 3). We compare HEC-RAS with LISFLOOD-FP using various grid sizes 25, 50 and 100m generated from a LiDAR DEM of 1m resolution. Moreover, along with the resampled DEMs we use the sub-grid capabilities of HEC-RAS by applying sub-grid terrain of 1m resolution within the 25, 50 and 100m sized meshes.

We explicitly focus on the fully 2D formulations for both models addressing the representation of the floodplain wave dynamics, i.e. no 1D component is included in the simulations (no

channel flow simulated). This is done in order to see the difference in the codes' ability to simulate inundation propagating over complex topography and an initially dry floodplain.

3. Study event and data used, models set-up and calibration

3.1. Study event and data

The event was characterized by a levee breach and consequent flooding of over 50 km² of the plain behind the dike within 48 hours causing significant population displacement, one death and economic losses in excess of 400 million Euro (D'Alpaos et al. 2014; Carisi et al. 2018). It occurred around 6:00 am on January 19 when a part of the levee in the right bank of Secchia River collapsed (see Figure 3). Although the water levels in the river did not exceed the designed embankment crest height, right after the breach the crest lowered by about 1m compared to the water elevation in the Secchia River. The conclusion driven from the post-event analysis is that the reason for the levee collapse was the activity of burrowing animals in the area (Vacondio et al. 2016; Orlandini et al. 2015).

Over the event the breach width reached nearly 100m and the inflow water volume that penetrated the floodplain reaching the municipalities of Modena, Bastiglia and Bomporto was estimated in 38.7·10x6 m³ (Figure 4). Previous studies showed that linear terrain irregularities strongly affected the flooding dynamics (Castellarin 2014; Hailemariam et al. 2014; Carisi et al. 2018; Domeneghetti 2014). Post event field surveys made by the local authorities together with other publicly available data (photographs, videos and Google Earth images) provided us with the water marks (maximum water depths) at certain points. The study of Horritt et al. (2010) shows that the post-event collection and evaluation of the water marks and wreck marks is not always matches the actual maximum values. Field measurement methods and their interpretation done by surveying groups, approximations of the elevation of water marks acquired from images may produce uncertainties. Horritt et al. (2010) reports that accuracy range in such estimations is likely to be up to 0.5m, which could be a potential source of errors. In order to check the liability of the observed water marks, we plotted them in relation to the 1m LiDAR DEM in order to see if there are water surface elevation outliers (points in closer vicinity with the large difference in depth). We looked at their weighted average and observations difference and removed the outliers (>0.5m). As the result we further used 46 water mark points to validate the maximum simulated water depth. We, however, left the

points in very close distance from each other (<50m) in order to look at the models' performance with different sub-grid configurations.

Official reports recorded vast damage in the small town of Bomporto (Carisi et al. 2018). During the event the area within the embankment was completely flooded (Figure 5). We selected the area surrounding this particular town due to its complex and highly anthropogenically altered terrain (e.g. minor levees, embankments, irrigation and drainage channel networks, etc.) to test how the models were able to reproduce the propagation of inundated extent in such topography. The water marks are located within the populated areas; therefore they are concentrated within the affected settlements of Bastiglia and Bomporto and the close vicinity around them. Fewtrell et al. (2008) in their study explicitly showed that the 2D models behaviour is strongly affected by the heterogeneity of the urban fabric and requires a very fine mesh to represent the building dimensions. Thus, we are particularly interested how the selected models will perform in built-up zones. We used these data to validate the models by comparing them to maximum water depths observed during the event (Carisi et al. 2018). The study by Carisi et al. (2018) reproduced the Secchia event simulating the inundation dynamic.. The simulations of Carisi et al. (2018) were based on the higher resolution 1m LiDAR DEM with unstructured mesh, whose faces ranged in size from 1 to 200m in more homogenous zones. The linear terrain irregularities were explicitly represented. The official reports done on the post-event field data collection and simulations made possible to reconstruct the flood extent as detailed as possible (D'Alpaos et al. 2014). The simulations showed a high correspondence with the maximum flood extent records (up to 0.9 in terms of measure of fit) (Carisi et al. 2018).

3.2. Models configuration and set-up

Previous modelling studies of the January 2014 inundation event showed that the topography of the area strongly controls the model performance (Vacondio et al. 2016; Carisi et al. 2018). As our interest is to show how the models behave at large scales, we considered downscaling the 1m LIDAR DEM to 25, 50 and 100 meters by taking the mean of the pixels' value. The vertical accuracy of the bare earth DEM is ± 0.15m (Geoportale Nazionale 2017). The study of Savage et al. (2016) on regional flood modelling showed that resolution coarser than 100m decreases the reliability of the model's outcomes, therefore, we avoided using lower resolutions. The same study showed that probabilistic flood mapping does not benefit much from resolution higher than 50m. Nevertheless, as our study is specifically focused on

heterogeneous topography, we intentionally included a 25m DEM in order to have a more profound comparison of the two different models.

The flow leaving the breach was estimated based on the difference between observed discharge hydrographs 200m upstream and 200m downstream along the reach (see Figure 4) (Vacondio et al. 2016).

Both models were constructed adopting the same hydraulic loads. The upstream boundary condition was represented by the discharge flowing through the levee breach and it was fixed in each simulation as a point (a pixel) located at the failure location. The breach width was set in all simulations equal to 100m, simultaneously involving 1, 2 and 4 pixels in the simulations using 100m, 50m and 25m resolutions, in this order. The inflow hydrograph was represented by the values retrieved from the studies of Carisi et al. (2018), Vacondio et al. (2016) and Orlandini et al. (2015). In order to avoid possible errors coming from different widths of the upstream boundary (levee breach breadth), we insured that the water marks are located further downstream from the inflow location.

We referred to the CORINE Land Cover (EEA 2007) and OpenStreetMap (Contributors OSM 2012) data sets for classifying land-use in the study area, which we represented in the models using spatially varying roughness coefficients. In particular, we adopted a subdivision of the study area into 2 main classes: built up (i.e. urban and industrial zones) and rural (i.e. all other land-use types mostly represented as agricultural fields) areas.

Fully 2D HEC-RAS was used and tested with and without its sub-grid function capability with structured mesh cell sizes of 25x25, 50x50 and 100x100m based on the 1m LiDAR DEM. Structured mesh selection significantly decreases the model set-up time and does not require additional data (i.e. linear infrastructure outlines) as is the case for configuration of an unstructured mesh. This is of a high importance for large-scale simulations, where such details might be unavailable or their implementation would require significant effort.

The meshes were also used with the corresponding aggregated DEM (25x25 mesh with 25m DEM resolution, 50x50 mesh with 50m DEM resolution, 100x100 mesh with 100m DEM resolution). Overall, we apply 9 mesh/terrain configurations as indicated in Table 1.

3.3. Models calibration

The models were calibrated using roughness coefficients for HEC-RAS and LISFLOOD-FP at 25m resolution. We looked into previous research and post-event surveys done to describe and analyse this event. In particular, we considered the publication of Carisi et al. (2018) and the accurate reconstruction of the flood extent reported therein. We compared the maximum flood

extent resulting from the models with the reference flood extent from Carisi et al. (2018) by means of a well-known method to compare binary maps (wet and dry areas) of the simulated and observed extents using a performance measure (Schumann et al. 2009):

$$F = \frac{\mathrm{A}}{\mathrm{A+B+C}} * 100 \quad (8)$$

Where A is the area correctly predicted as flooded (wet in both observed and simulated), B is the area overpredicting the extent (dry in observed but wet in simulated) and C is the underpredicted flood area (wet in observed but dry in simulated). F defined in (8) varies between 0 and 100%, where 100% corresponds to a perfect match between the modelled extent and the reference inundation map (Horritt and Bates 2002).

Calibration consisted of varying the Manning's roughness coefficient, *n*, of rural areas from 0.03 to $0.2m^{-1/3}$s, by $0.005m^{-1/3}$s increments, while keeping *n* of urbanised zones constant ($0.3m^{-1/3}$s, (Syme 2008)) and referring to the land-use description resulting from CORINE Land Cover data (EEA 2007) and OpenStreetMap (2012). So, for each simulation we would use one roughness coefficient for rural and one for urban areas. LISFLOOD-FP resulted in the highest *F* value (81%) for a floodplain roughness coefficient $n = 0.155m^{-1/3}s$; with *F* varying between 73% for $n = 0.030m^{-1/3}s$ and 77% for $n = 0.200m^{-1/3}s$. HEC-RAS showed similar performance, maximum F value is equal to 78% at $n = 0.195m^{-1/3}s$, however *F* values plateau at 78% for *n* values larger than $0.185m^{-1/3}s$. For the further analysis we selected the value of $0.195m^{-1/3}$. These values ($0.195m^{-1/3}$ for rural and $0.3m^{-1/3}$ for urban areas) do not reflect the actual vegetation/soil cover in the area, they are aimed at compensating for the possible errors coming from the overall flooding extent used to calibrate the model and possible limitations related to the inability of the terrain to capture the linear features, which played a crucial role in routing the flow. Also, we calibrated both models at 50m and 100m resolution, obtaining optimal values of the calibration parameters that differed from the optimal values at 25m resolution by less than 1%. Therefore, we decided to use uniform optimal values for all resolutions.

Both models were validated against 46 water marks (see e.g. Figure 5) for which the maximum water depth (m) was surveyed in the event aftermath (water marks, post-event surveys, interviews and geolocating the marks using aerial and ground photographs). Dry simulated points were given zero value. Comparison was performed by means of Root Mean Square Error (RMSE). All simulations were performed on the 4 cores with the Intel Core i7 3.60 GHz CPU, 64 GB RAM.

4. Results

From Figure 6 we can see that the overall performance in terms of inundation extent (i.e. F values defined as in (8)) of LISFLOOD-FP is slightly better than HEC-RAS. The 25m LISFLOOD-FP simulation (L25) was able to correctly simulate 81% of the flooding extent, while the 50m LISFLOOD-FP simulation (L50) was as good as the HEC-RAS simulation with 1m sub-grid terrain (78%). All other configurations produced almost identical results, with an F value of ~77%. However, the spatial pattern of the flooded areas differs for all configurations (Figure 6).

Together with the analysis of the overall inundation extent, the performance of each model was scrupulously assessed relative to specific areas in the towns of Bomporto and Bastiglia. Figure 5 illustrates the observed extent and the location of focus areas. From Figure 7 we can see that the LISFLOOD-FP model was able to correctly simulate the maximum flood extent in Bomporto for the fine resolution of 25m, while with other LISFLOOD-FP resolutions the same results were not achieved. The red line in these maps demarcates the observed inundation extent, so we can see that the L25 configuration output is in good agreement with the observations (the flood propagated to the observed inundation boundary and covered all water marks). The LISFLOOD-FP 50m and 100m simulations (L50 and L100) did not properly simulate the flood propagation in this area. The water marks display the accuracy of predicted water levels in relation to the observations. Figure 7 shows that the flood extent simulated by HEC-RAS for 25, 50 and 100m mesh sizes with 1m sub-grid terrain was consistent with the observations, especially the larger meshes of 50 and 100m. The HEC-RAS models without sub-grid terrain (HR25_25, HR50_50 and HR100_100) were unable to simulate the flood wave propagation in the Bomporto focus area.

As for the other focus area, from Figure 8 we can see that the flood extent in Bastiglia produced by all LISFLOOD-FP resolutions is in-line with the observed flood extent. The L25 configuration was more successful in reproducing the flood extent over the control areas, while the L50 and L100 models just slightly underestimate the flood boundaries (see Figure 7 and Figure 8). HEC-RAS coarser grid simulations (25, 50 and 100m sub-grid), similar to LISFLOOD-FP (50 and 100m), produce plausible results in terms of the inundation extent. The accuracy decreases with increasing mesh size. The HEC-RAS configurations using sub-grid terrain of 1m resolution struggle to produce a continuous inundation pattern, resulting in numerous dry islands.

Figures 7 and 8 display the water marks and the colour indicates on the level of absolute difference between simulated and surveyed maximum water levels through a red (underestimation) to dark green (overestimation) colour scale. The largest difference is especially visible in Bomporto focus area (up to 1.8 meters), as most of the simulations did not succeed in inundating the town. While in Bastiglia such difference is less pronounced. There, the values vary between 0.1m and 1.2m. General tendency for all simulations is underestimation of the water depth values at water marks.

In addition, we compared observed and simulated maximum water levels using RMSE. Overall, the best results (see Table 3) are of L25 configuration (0.61m). Same performance was obtained from HEC50_1 (0.62m). The results from L50 and L100 are similar to those gotten from HR25_25, HR50_50 and HR100_100 (0.79-0.84m), while the other high-resolution sub-grid terrain of HEC-RAS produced somewhat better outcomes 0.71m.

Another important factor to be considered in the mesh size and DEM resolution evaluation is the computation time. From Figure 9 we can see that in all simulations LISFLOOD-FP was significantly faster than HEC-RAS, no numerical instabilities reported. For instance, the 100m resolution HEC-RAS simulation lasted about a minute, while the 25m mesh size simulation with this model would take about 45 minutes (See Figure 9).

LISFLOOD-FP was about 20 times faster than HEC-RAS for the same grids and time step (L50 was 1 min 20 sec computation time, HR50_1 was 25 min computation time). HEC-RAS of 25m resolution and 25m subgrid terrain is faster than the same resolution with 25m terrain, but this difference become less evident for large mesh. HEC-RAS of 100m large mesh and 1m subgrid resolution is 4 times slower than HR100_100, it means that considering high performance (overall extent 78% accuracy and 0.71m RMSE at water marks) HR100_1 is the best choice in HEC-RAS simulations. When 1m subgrid is implemented in HEC-RAS simulations, the model performs similarly in terms of flood extent (See Table 3), however the computation time can be drastically decreased by using large mesh (HR100_1). L25 has shown best performance in terms of flood extent and water depth at selected control points, however it is 2 times slower than HR100_1.

5. Discussion

The two codes of different complexity and terrain resolution, used in this study, strongly affect the quality of the outputs. Diffusion wave model (HEC-RAS) and inertial formulation of the shallow water equation (LISFLOOD-FP) are distinct in different ways. The ability of HEC-

RAS to include the sub-grid bathymetry component makes it effective in terms of representation of topographic details by computing more informative property tables for each cell face. LISFLOOD in turn, operates with the rectangular mesh of the same resolution as the input terrain raster.

5.1. Performance comparison

As it was outlined in the Results section, the structured regular mesh of both models is able to reproduce the flooding event with sufficient correspondence with observations and capture the overall inundation extent and water depth marks at selected water marks. The mesh size played a great role in the accuracy of the outputs of LISFLOOD-FP; the 25m grid model performed somewhat better than coarser girds considering the inundation boundary. One of the main reasons for such performance is the ability of the finer resolution models to capture more terrain details and route the flow into the right direction considering depressions and the elevations of the relief. The flood extent of the 50 and 100m models (L50 and L100, respectively) were virtually similar, differing by only 1% from each other in terms of the measure of fit value *F*. HEC-RAS, in turn had comparable results across the resolutions and sub-grid terrain configurations considering flood extent in the whole study area; nevertheless, compared to LISFLOOD-FP (L25), the *F* value is slightly less accurate. This is of specific importance for areas with complex topography. Overall extent differences between best performing L25 and the rest of configurations, however, are minimal. This can be explained by rather confined area, which is shaped by the embankments of the Secchia River from the west and another river from the east, moreover the northern boundary is also well-pronounced and acts as a barrier to the flood water preventing it propagating further north. Therefore, we suggest that the terrain configuration explains the similar performance of the models (77-78% accuracy, apart from L25 with 81% accuracy). This also confirms the previous findings that inundation extent over larger areas can be properly identified with the low-resolution datasets (in our case 50 or 100m), with additional benefit of lower computational costs (Savage et al. 2016). Such findings can be relevant for areas with similar terrain configurations regardless geographical location.

However, as predicted the behaviour of the models in the focus areas had diverse patterns. For instance, HR50_1 and HR100_1 were able to represent the inundation boundaries in Bomporto fairly well, unlike in Bastiglia (see Figure 7 and Figure 8). While LISFLOOD-FP was more accurate at high resolution of 25m compared to 50 and 100m. L25 performed strikingly better than HR25_25 both overall and in the two focus areas (i.e. Bomporto and Bastiglia). We explicitly highlight such results, as L25 provided best outcomes in terms flood extent and water

depth across all selected configurations (see Table 2 and Table 3). We suggest that this outcome of both models is strongly related to their ability to simulate floods in built-up areas with given resolution. It is known that the towns of Bomporto and Bastiglia are not only represented by urban fabric but also surrounded by a network of smaller channels and embankments, which in case of 2014 flood event played a crucial role in the inundation dynamics.

One of the similarities between both models is the performance of the 50m and 100m LISFLOOD-FP and HEC-RAS models when sub-grid terrain resolutions are not considered for the latter code. For instance, by applying configurations L50 and HR50_50 we attained rather comparable inundation patterns in Bastiglia (see Figure 8) and almost identical in Bomporto (see Figure 7).

The water mark errors evaluated in the current study show how models represented water depth spatially. A point that deserves attention is the vertical accuracy of the input and calibration data. As was discussed earlier, the vertical accuracy of the used LiDAR dataset (±0.15m) and the observed data (±0.5m), is a subject of uncertainties. Looking at the differences between observed and simulated water mark values, we may suggest that the RMSEs are within the input data error range. Despite eliminating the outliers, we cannot be 100% confident that the values perfectly match the reality. Therefore, here we treat the results as a relative comparison between the two models rather than compare absolute observed and simulated values. In addition, the points also serve as an indicator to evaluate the simulations, where the water marks did not get inundated. Overall, in terms of RMSE HEC-RAS with 1m subgrid terrain for all resolutions was better compared to coarser terrains (approx. 0.13m difference in terms of RMSE between HEC-RAS 1m sub-grid and coarse sub-grids, including LISFLOOD-FP simulations). The only exception is LISFLOOD-FP of 25m resolution, which was comparable to high-detailed sub-grid of HEC-RAS (RMSE error equal to 0.61 and 0.62m correspondingly). We suggest that such performance can be reasoned by the fact that most of the points are located within rather short distance (up to 200m) on heterogeneous terrain, meaning the water depth points varied by over 1m. At Bomporto and Bastiglia focus areas, some points were located within short distance of 30-40m, which was far denser than the resolution of the underlying terrains (50-100m). Therefore, HEC-RAS on 1m sub-grid performed the best due to its ability to operate with highly-detailed terrain compared to other configurations with coarse sub-grids (both, LISFLOOD-FP and HEC-RAS).

The differences in terms of computation time outlined in the Results section are crucial for instance for calibration and running Monte Carlo simulation scenarios, especially, if we intend to extrapolate this performance parameter to the larger-scale studies. Therefore, we may draw

a suggestion, that flood mapping for geographically large areas can still be performed with the coarser grids (50 or 100 meters) and produce reasonable results to identify the flood risk hotspots. Such hotspots can be then analysed using high-resolution datasets. In HEC-RAS configurations the use of high-resolution (1m) sub-grid outperforms those of the same resolution as size of the mesh (25, 50, 100m). However, the computational costs for 1m sub-grid increases. The modeller should select among the two options in relation to the mesh size, when the mesh size is small (25m) the difference in computation time is significant. On the other hand, when the mesh size is larger, the difference in terms of computation time among two becomes smaller. 1m sub-grid becomes more beneficial to be used in terms of computation time, as it additionally shows high performance.

Nevertheless, speaking of large-scale simulations, we expect that smaller areas complicated by highly heterogeneous terrain but with the potential for large socio-economic impacts (as it is in Bomporto) will still be misrepresented and wrongly estimated. As shown in the example of this study, the resolution of the topographic description is not the only key factor; another element of paramount importance is the ability of the model mesh/grid to correctly capture critical terrain features which determine the flood wave propagation. This aspect becomes particularly crucial when simulating floods over heavily anthropogenically altered floodplains, as it was the case in our study.

The solution of the problem can be assisted by performing a bottom up assessment, where the most vulnerable and susceptible areas are initially considered in hazard modelling, such as was done in the current study. As it was known which areas were impacted the most, we particularly focused on the model behaviour in these regions. It helped us to attain better performance based on the study of Carisi et al. (2018) for the January 2014 event. In probabilistic assessment, these areas can be particularly outlined by intentionally focusing on the locations with high concentration of population/assets, meaning, more attention should be given to analyse flood characteristics in the calibration stage. By doing this, we may reduce uncertainties related to the identification of hotspots.

5.2. Limitations

One of the main issues for the HEC-RAS applications is the way in which the model distributes the water within a mesh cell. The volume-elevation curve drawn for each cell-face while pre-processing does not recognise the exact location of the higher/lower ground of the sub-grid terrain. In case of rectangular mesh, when the cell faces are not aligned with the elevated linear features, they are not captured into the property tables. We may therefore observe a leaking

effect (Figure 10), or the opposite way when the model would not recognise the obstacles for the flow and route it further onto a neighbouring cell. This is a known limitation, previously observed in the used version of HEC-RAS 5.0 (Goodell 2015). In our case, we noticed that there is a certain amount of hydraulically disconnected flooded areas. Moreover, this effect is particularly obvious in the simulations with coarser sub-grid terrains. Some areas (Figure 10) simulated as flooded are, however disconnected from the main inundated area. This might be a limitation in the calculations of the flood extent and, in some cases, the distribution of local water depth values. This problem is normally solved by refining the mesh with the breaklines, reducing the mesh sizes along such linear irregularities, however, as explained above, the current study did not look into such property.

Inundation boundaries produced by LISFLOOD-FP should be also taken with great care, as the model operates with a raster grid, and the water is distributed equally across the whole cell. For coarse grid resolutions (i.e. pixel size equal or larger than 100m) it might thus misestimate the flood extent. In areas with complex topography, it is necessary to include important terrain features into the model. Due to the fact that LISFLOOD-FP simulates 4 directional water propagation at each cell face (i.e., D4 routing), the linear irregularities captured by L25 configuration (see Figure 11) would actually be sufficient to limit the flood propagation over such an elevation distribution. We suggest that this simplification of LISFLOOD-FP in case of high-elevation fine linear terrain features (i.e. levees, embankments, see Figure 11 light green cells) could help to route the water in the right direction and not to “leak” through the embankments. Nevertheless, the same peculiarity would restrain the water propagation in lower-elevation fine linear terrain features (i.e. rivers, canals, drainage networks) (blue cells in Figure , area near Bomporto). The same point applies to structured grid of HEC-RAS.

By having 25m mesh cell size (smallest in this case) it is not always possible to capture important local topographical features, such as embankments, small channels, etc., especially, when the linear features are significantly narrower than the model resolution. The known and widely used practice to include the actual terrain heights (levees, embankments, etc.) by “burning” them into the coarser terrain enables capturing such features, even when their width is smaller than the terrain resolution and mesh size. We intentionally avoided such option to see how the models would respond to the simplified approach of terrain pre-processing. Supposedly, on the geographically larger scale such manipulation when the complex and dense network of narrow levees in a specific area are “burnt” in the terrain, may not be always feasible and/or effective. Especially, in cases when such modifications would greatly affect the storage volume of floodplains (i.e. when 100x100m raster cell is given the height of the much narrower

feature of 10m breadth). Moreover, this is certainly a challenging task for the areas, which are not covered with LIDAR data acquisition and areas with poor data availability and quality in general.

6. Conclusions

Due to the specific nature of the event described in this study and the growing use of fully 2D codes for flood modelling, we evaluated and compared the performance of the well-known HEC-RAS and LISLOOD-FP models for a floodplain with a complex and highly anthropogenically altered topography. The aim of the study was to see how the models of different complexity with given terrain resolution reproduce the flooding event and how accurate the results are. The resolutions were rather coarse for the given study area as our main goal was to identify the potential of the codes and mesh dimensions to simulate events over large regions.

One of the conclusions from the study is that 50m resolution for describing terrain with complex linear features is a reasonable compromise between output accuracy and computation time for LISFLOOD-FP model, while HEC-RAS optimum solution would be the configuration of 1m subgrid terrain and 100m mesh size.. This experience may contribute to simulations performed at catchment scales designed to capture large-scale system behaviour. Specific floodplain morphology may serve as water storage areas during flooding events and hence, lower the risks in the downstream part of the catchment.

Another point is the complexity of the modelling schemes. Raster-based LISFLOOD-FP was more efficient at representing overall flood extent and water depth at water marks, while HEC-RAS performed better at representing spatial distribution details (i.e. inundation boundary) considering given terrain (due to its high-resolution sub-grid feature). Therefore, a selection of the modelling scheme and resolution should be carefully considered depending on the purpose of each given case study.

Finally, a topical issue in 2D code usage for large-scale simulations using high-resolution datasets is computational cost. As mentioned above, this can be significantly advanced by using GPU version of the codes. In this study we highlight the computational advantage of the inertial formulation of the shallow water LISFLOOD-FP model compared to diffusion wave HEC-RAS. This study shows that codes with simplified physics are a necessary tool for probabilistic/preliminary flood risk assessment. Moreover, by including high-resolution sub-grid (HEC-RAS with 1m terrain) we obtain more detailed hazard maps even for large meshes (i.e. 25, 50, 100), however, sacrificing the computational time. When comparing the overall

performance of L25 and HR100_1, the latter one is two times faster, however L25 showed somewhat better results in flood extent and water depth representation.

Nevertheless, we suggest that more complex tools (i.e. full momentum shallow water codes) have their place in local-scale studies to provide hyper-detailed hydrodynamic modelling. Moreover, future work should consider the cases when the channel flow simulation is included in the model. Such advances will shed more light on the application of 2D models of different complexity.

References

Alfieri, L.; Bisselink, B.; Dottori, F.; Naumann, G.; Roo, A. de; Salamon, P. et al. (2017): Global projections of river flood risk in a warmer world. In *Earth's Future* 5 (2), pp. 171–182. DOI: 10.1002/2016EF000485.

Alfieri, L.; Burek, P.; Feyen, L.; Forzieri, G. (2015): Global warming increases the frequency of river floods in Europe. In *Hydrol. Earth Syst. Sci.* 19 (5), pp. 2247–2260. DOI: 10.5194/hess-19-2247-2015.

Alfieri, L.; Salamon, P.; Bianchi, A.; Neal, J.; Bates, P.; Feyen, L. (2014): Advances in pan-European flood hazard mapping. In *Hydrol. Process.* 28 (13), pp. 4067–4077. DOI: 10.1002/hyp.9947.

Almeida, Gustavo A. M. de; Bates, Paul (2013): Applicability of the local inertial approximation of the shallow water equations to flood modeling. In *Water Resour. Res.* 49 (8), pp. 4833–4844. DOI: 10.1002/wrcr.20366.

Apel, H.; Aronica, G. T.; Kreibich, H.; Thieken, A. H. (2009): Flood risk analyses—how detailed do we need to be? In *Nat Hazards* 49 (1), pp. 79–98. DOI: 10.1007/s11069-008-9277-8.

Arnell, Nigel W.; Gosling, Simon N. (2016): The impacts of climate change on river flood risk at the global scale. In *Climatic Change* 134 (3), pp. 387–401. DOI: 10.1007/s10584-014-1084-5.

Aronica, G.; Bates, P. D.; Horritt, M. S. (2002): Assessing the uncertainty in distributed model predictions using observed binary pattern information within GLUE. In *Hydrol. Process.* 16 (10), pp. 2001–2016. DOI: 10.1002/hyp.398.

Bates, P.; Horritt, M. S.; Fewtrell, T. J. (2010): A simple inertial formulation of the shallow water equations for efficient two-dimensional flood inundation modelling. In *Journal of Hydrology* 387 (1-2), pp. 33–45. DOI: 10.1016/j.jhydrol.2010.03.027.

Bates, P.D; Roo, A.P.J de (2000): A simple raster-based model for flood inundation simulation. In *Journal of Hydrology* 236 (1-2), pp. 54–77. DOI: 10.1016/S0022-1694(00)00278-X.

Brunner, G. W. (2016): HEC-RAS River Analysis System. Hydraulic Reference Manual. Version 5.0. HYDROLOGIC ENGINEERING CENTER DAVIS CA.

Büchele, B.; Kreibich, H.; Kron, A.; Thieken, A.; Ihringer, J.; Oberle, P. et al. (2006): Flood-risk mapping. Contributions towards an enhanced assessment of extreme events and associated risks. In *Nat. Hazards Earth Syst. Sci.* 6 (4), pp. 485–503. DOI: 10.5194/nhess-6-485-2006.

Carisi, F.; Schröter, K.; Domeneghetti, A.; Kreibich, H.; Castellarin, A. (2018): Development and assessment of uni- and multivariable flood loss models for Emilia-Romagna (Italy). In *Nat. Hazards Earth Syst. Sci.* 18 (7), pp. 2057–2079. DOI: 10.5194/nhess-18-2057-2018.

Castellarin, A. (2014): Evolving water resources systems. Understanding, predicting and managing water - society interactions. Wallingford, Oxfordshire: International Association of Hydrological Sciences (IAHS) Press (IAHS publication, 0144-7815, 364).

Contributors OSM (2012): OpenStreetMap. Available online at www.openstreetmap.org.

Coulthard, Tom J.; Neal, Jeff C.; Bates, Paul D.; Ramirez, Jorge; Almeida, Gustavo A. M. de; Hancock, Greg R. (2013): Integrating the LISFLOOD-FP 2D hydrodynamic model with the CAESAR model. Implications for modelling landscape evolution. In *Earth Surf. Process. Landforms* 38 (15), pp. 1897–1906. DOI: 10.1002/esp.3478.

D'Alpaos, L.; Brath, A.; Fioravante, V.; Gottardi, G.; Mignosa, P.; Orlandini, S. (2014): Relazione tecnico-scientifica sulle cause del collasso dell'argine del fiume Secchia avvenuto il giorno 19 gennaio 2014 presso la frazione San Matteo: Regione Emilia-Romagna, Bologna.

Di Baldassare, G.; Castellarin, A.; Molnar, P.; Brath, A. (2009): Probability-weighted hazard maps for comparing different flood risk management strategies. A case study. In *Nat Hazards* 50 (3), pp. 479–496. DOI: 10.1007/s11069-009-9355-6.

Di Baldassare, G.; Schumann, G. J.-P.; Bates, P. D.; Freer, J. E.; Beven, K. J. (2010): Flood-plain mapping. A critical discussion of deterministic and probabilistic approaches. In *Hydrological Sciences Journal* 55 (3), pp. 364–376. DOI: 10.1080/02626661003683389.

Dimitriadis, P.; Tegos, A.; Oikonomou, A.; Pagana, V.; Koukouvinos, A.; Mamassis, N. et al. (2016): Comparative evaluation of 1D and quasi-2D hydraulic models based on benchmark and real-world applications for uncertainty assessment in flood mapping. In *Journal of Hydrology* 534, pp. 478–492. DOI: 10.1016/j.jhydrol.2016.01.020.

Domeneghetti, A. (2014): Effects of minor drainage networks on flood hazard evaluation. In *Proc. IAHS* 364, pp. 192–197.

Domeneghetti, A.; Carisi, F.; Castellarin, A.; Brath, A. (2015): Evolution of flood risk over large areas. Quantitative assessment for the Po river. In *Journal of Hydrology* 527, pp. 809–823. DOI: 10.1016/j.jhydrol.2015.05.043.

Domeneghetti, A.; Vorogushyn, S.; Castellarin, A.; Merz, B.; Brath, A. (2013): Probabilistic flood hazard mapping. Effects of uncertain boundary conditions. In *Hydrol. Earth Syst. Sci.* 17 (8), pp. 3127–3140. DOI: 10.5194/hess-17-3127-2013.

EC (2007): Directive 2007/60/EC of the European Parliament and of the Directive 2007/60/EC of the European Parliament and of the Council of 23 October 2007 on the assessment and management of flood risks, Flood Directive, revised European Parliament and Council. In : Official Journal L 288.

EEA (2007): CLC2006 technical guidelines. Luxembourg: Publications Office (Technical report (European Environment Agency. Online), 17/2007).

Falter, D.; Vorogushyn, S.; Lhomme, J.; Apel, H.; Gouldby, B.; Merz, B. (2013): Hydraulic model evaluation for large-scale flood risk assessments. In *Hydrol. Process.* 27 (9), pp. 1331–1340. DOI: 10.1002/hyp.9553.

Fewtrell, T. J.; Bates, P. D.; Horritt, M.; Hunter, N. M. (2008): Evaluating the effect of scale in flood inundation modelling in urban environments. In *Hydrol. Process.* 22 (26), pp. 5107–5118. DOI: 10.1002/hyp.7148.

Geoportale Nazionale (2017): Progetto PST - Dati LiDAR. Available online at http://www.pcn.minambiente.it/mattm/progetto-pst-dati-lidar/.

Goodell, C. (2015): The RAS Solution 2015. 2D Mesh “Leaking”. Available online at http://hecrasmodel.blogspot.com/search/label/Leaking.

Haile, A. T.; Rientjes, T. H.M. (2005): Effects of LiDAR DEM resolution in flood modelling. A model sensitivity study for the city of Tegucigalpa, Honduras. In *Isprs wg iii/3, iii/4* 3, pp. 12–14.

Hailemariam, F. M.; Brandimarte, L.; Dottori, F. (2014): Investigating the influence of minor hydraulic structures on modeling flood events in lowland areas. In *Hydrol. Process.* 28 (4), pp. 1742–1755. DOI: 10.1002/hyp.9717.

Horritt, M. S.; Bates, P. D. (2002): Evaluation of 1D and 2D numerical models for predicting river flood inundation. In *Journal of Hydrology* 268 (1-4), pp. 87–99. DOI: 10.1016/S0022-1694(02)00121-X.

Horritt, M. S.; Bates, P. D.; Fewtrell, T. J.; Mason, D. C.; Wilson, M. D. (2010): Modelling the hydraulics of the Carlisle 2005 flood event. In *Proceedings of the Institution of Civil Engineers - Water Management* 163 (6), pp. 273–281. DOI: 10.1680/wama.2010.163.6.273.

Hunter, N. M.; Bates, P. D.; Neelz, S.; Pender, G.; Villanueva, I.; Wright, N. G. et al. (2008): Benchmarking 2D hydraulic models for urban flooding. In *Proceedings of the Institution of Civil Engineers - Water Management* 161 (1), pp. 13–30. DOI: 10.1680/wama.2008.161.1.13.

Kundzewicz, Z. W.; Kanae, S.; Seneviratne, S. I.; Handmer, J.; Nicholls, N.; Peduzzi, P. et al. (2013): Flood risk and climate change. Global and regional perspectives. In *Hydrological Sciences Journal* 59 (1), pp. 1–28. DOI: 10.1080/02626667.2013.857411.

Lehner, B.; Döll, P.; Alcamo, J.; Henrichs, T.; Kaspar, F. (2006): Estimating the Impact of Global Change on Flood and Drought Risks in Europe. A Continental, Integrated Analysis. In *Climatic Change* 75 (3), pp. 273–299. DOI: 10.1007/s10584-006-6338-4.

Liu, Z.; Merwade, V.; Jafarzadegan, K. (2019): Investigating the role of model structure and surface roughness in generating flood inundation extents using one- and two-dimensional hydraulic models. In *Journal of Flood Risk Management* 12 (1), e12347. DOI: 10.1111/jfr3.12347.

Milly, P. C. D.; Wetherald, R. T.; Dunne, K. A.; Delworth, T. L. (2002): Increasing risk of great floods in a changing climate. In *Nature* 415 (6871), pp. 514–517. DOI: 10.1038/415514a.

Moel, H. de; van Alphen, J.; Aerts, JCJH (2009): Flood maps in Europe–methods, availability and use. In *Natural Hazards and Earth System Sciences* 9 (2), pp. 289–301.

Morsy, M. M.; Goodall, J. L.; O'Neil, G. L.; Sadler, J. M.; Voce, D.; Hassan, G.; Huxley, C. (2018): A cloud-based flood warning system for forecasting impacts to transportation infrastructure systems. In *Environmental Modelling & Software* 107, pp. 231–244. DOI: 10.1016/j.envsoft.2018.05.007.

Munich RE (2015a): Loss events worldwide 1980–2014, 10 costliest events ordered by overall losses. In *Annual statistic. Munich*.

Munich RE (2015b): NatCatSERVICE Loss Events Worldwide 1980–2014. In *Munich Reinsurance, Munich, Germany*.

Neal, J.; Villanueva, I.; Wright, N.; Willis, T.; Fewtrell, T.; Bates, P. (2012): How much physical complexity is needed to model flood inundation? In *Hydrol. Process.* 26 (15), pp. 2264–2282. DOI: 10.1002/hyp.8339.

Néelz S.; Pender G. (2013): Benchmarking the Latest Generation of 2D Hydraulic Flood Modelling Packages. Report SC120002. Environment Agency. Environment Agency, Horison House, Deanery Road,. Available online at http://publications.environmentagency.gov.uk, checked on 12/19/2018.

Orlandini, S.; Moretti, G.; Albertson, J. D. (2015): Evidence of an emerging levee failure mechanism causing disastrous floods in Italy. In *Water Resour. Res.* 51 (10), pp. 7995–8011. DOI: 10.1002/2015WR017426.

Sampson, C. C.; Smith, A. M.; Bates, P.; Neal, J.; Alfieri, L.; Freer, J. E. (2015): A high-resolution global flood hazard model. In *Water resources research* 51 (9), pp. 7358–7381. DOI: 10.1002/2015WR016954.

Savage, J. T. S.; Bates, P.; Freer, J. E.; Neal, J.; Aronica, G. (2016): When does spatial resolution become spurious in probabilistic flood inundation predictions? In *Hydrol. Process.* 30 (13), pp. 2014–2032. DOI: 10.1002/hyp.10749.

Schumann, G. J.-P.; Bates, P.; Horritt, M. S.; Matgen, P.; Pappenberger, F. (2009): Progress in integration of remote sensing–derived flood extent and stage data and hydraulic models. In *Rev. Geophys.* 47 (4), RG2002. DOI: 10.1029/2008RG000274.

Schumann, G. J.-P.; Stampoulis, D.; Smith, A. M.; Sampson, C. C.; Andreadis, K. M.; Neal, J.; Bates, P. (2016): Rethinking flood hazard at the global scale. In *Geophys. Res. Lett.* 43 (19), 10,249–10,256. DOI: 10.1002/2016GL070260.

Syme, W. J. (2008): 9th National Conference on Hydraulics in Water Engineering. Hydraulics 2008. Barton, A.C.T.: Engineers Australia.

Tayefi, V.; Lane, S. N.; Hardy, R. J.; Yu, D. (2007): A comparison of one- and two-dimensional approaches to modelling flood inundation over complex upland floodplains. In *Hydrol. Process.* 21 (23), pp. 3190–3202. DOI: 10.1002/hyp.6523.

Teng, J.; Jakeman, A. J.; Vaze, J.; Croke, B.F.W.; Dutta, D.; Kim, S. (2017): Flood inundation modelling. A review of methods, recent advances and uncertainty analysis. In *Environmental Modelling & Software* 90, pp. 201–216. DOI: 10.1016/j.envsoft.2017.01.006.

Vacondio, R.; Aureli, F.; Ferrari, A.; Mignosa, P.; Dal Palù, A. (2016): Simulation of the January 2014 flood on the Secchia River using a fast and high-resolution 2D parallel shallow-water numerical scheme. In *Nat Hazards* 80 (1), pp. 103–125. DOI: 10.1007/s11069-015-1959-4.

Vacondio, R.; Dal Palù, A.; Mignosa, P. (2014): GPU-enhanced Finite Volume Shallow Water solver for fast flood simulations. In *Environmental Modelling & Software* 57, pp. 60–75. DOI: 10.1016/j.envsoft.2014.02.003.

Figure 1. RasMapper representation of 2m sub-grid DEM and 25m mesh cell size of HEC-RAS 2D (adapted from Brunner (2016)).

Figure 2. Cell face terrain data (left) and schematic representation of A (area) – H (elevation) relationship reproduced with the Property Table (right) (adapted from Brunner (2016)).

Figure 3. Breach location and flow direction during the event.

Figure 4. Outflowing discharge at the levee breach point over time (adopted from D'Alpaos et al. 2014).

Figure 5. Observed flood extent, hotspot focus areas (green and red boxes) and water marks (control points). Green box captures the inundation in Bastiglia; the red box shows the inundation extent in Bomporto.

Table 1. Simulation configurations

Mesh Resolution	LISFLOOD	HEC RAS 1m sub-grid terrain resolution	HEC RAS 25/50/100m sub-grid terrain resolution
25	L25	HR25_1	HR25_25
50	L50	HR50_1	HR50_50
100	L100	HR100_1	HR100_100

Figure 6. Overall simulated extent for all configurations (blue), compared to the observed extent (red outline)

Figure 7. LISFLOOD-FP and HEC-RAS flood extent for different configurations at Bomporto (red box in Figure 5). Water depth difference (m) between predicted and observed at water mark points.

Figure 8. LISFLOOD-FP and HEC-RAS flood extent for different configurations at Bastiglia (green box in Figure 5). Water depth difference (m) between predicted and observed at water marks.

Table 2. Measure of Fit F (in %), inundation extent accuracy.

Mesh size [m]	LISFLOOD-FP	HEC-RAS 1m sub-grid	HEC-RAS 25/50/100m sub-grid
25	81	78	78
50	78	78	77
100	77	78	77

Table 3. RMSE [m] of the water depth at water marks

Mesh size [m]	LISFLOOD-FP	HEC-RAS 1m sub-grid	HEC-RAS 25/50/100m sub-grid
25	0.61	0.69	0.79
50	0.80	0.62	0.80
100	0.82	0.71	0.84

Figure 9. Approximate computation time of HEC-RAS and LISFLOOD-FP configurations

Figure10. Leakage effect of HEC-RAS sub-grid mesh examples of HR100_100 (left), HR25_1 (right). Larger ponds of water in both images are disconnected from the inundation extent.

Figure 11. 25m resolution DEM. Dark blue - canal, light green – levee.

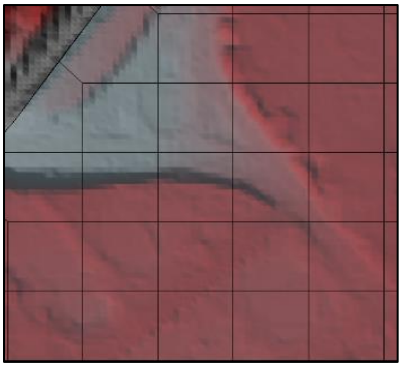

Figure 1. RasMapper representation of 2m sub-grid DEM and 25m mesh cell size of HEC-RAS 2D (adapted from Brunner (2016)).

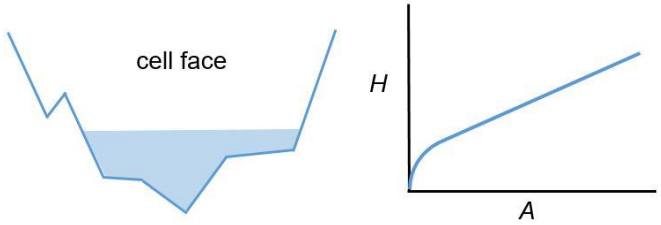

Figure 2. Cell face terrain data (left) and schematic representation of A (area) – H (elevation) relationship reproduced with the Property Table (right) (adapted from Brunner (2016)).

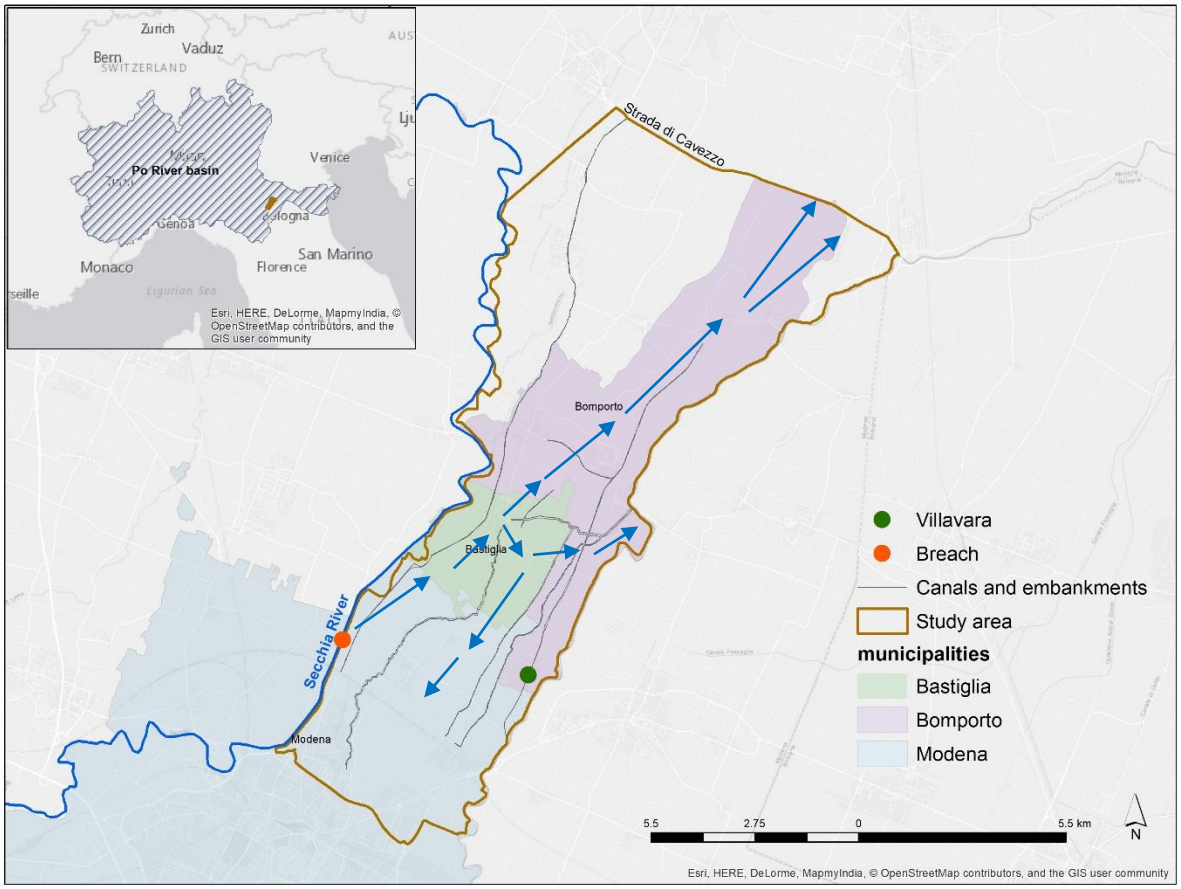

Figure 3. Breach location and flow direction during the event.

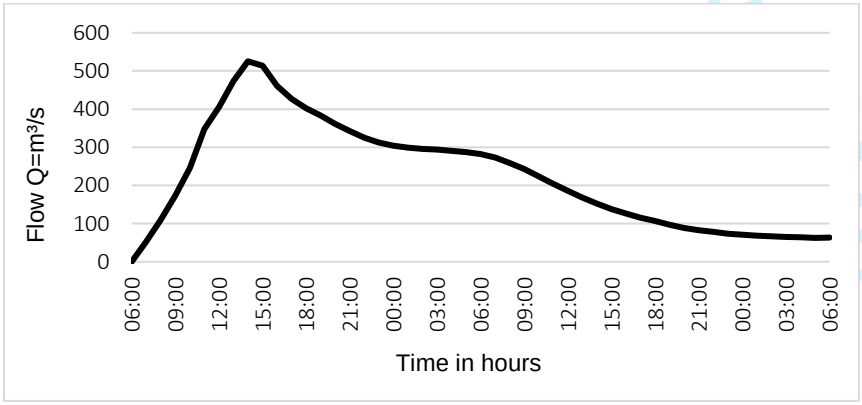

Figure 4. Outflowing discharge at the levee breach point over time (adopted from D'Alpaos et al. 2014).

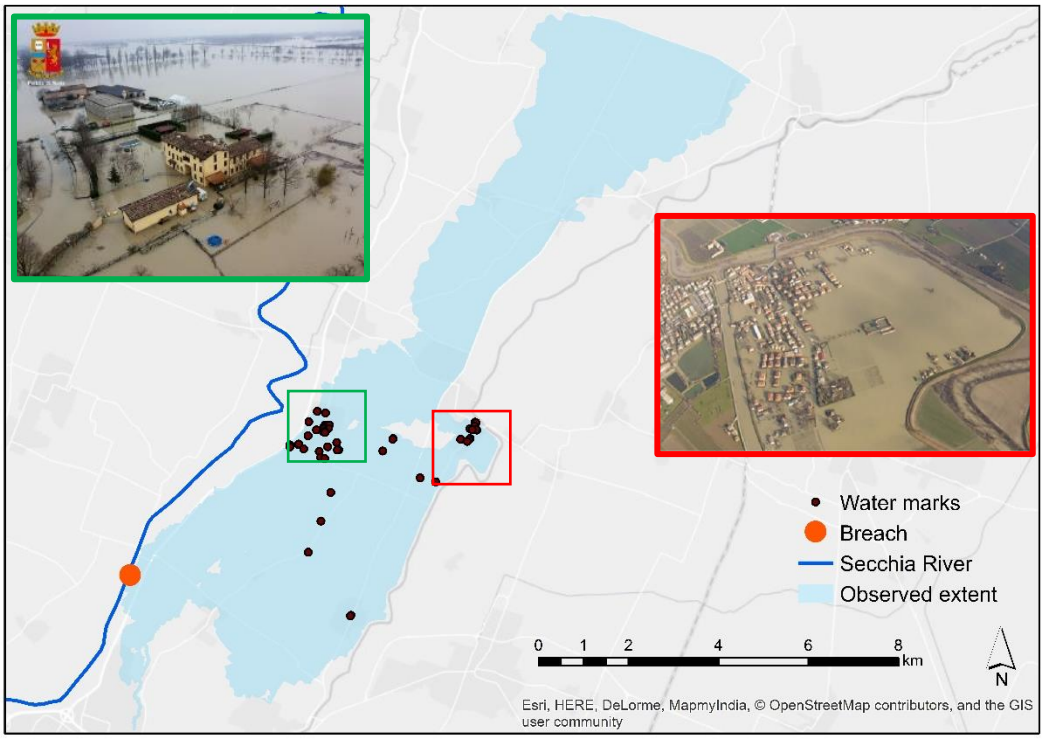

Figure 5. Observed flood extent, hotspot focus areas (green and red boxes) and water marks (control points). Green box captures the inundation in Bastiglia; the red box shows the inundation extent in Bomporto.

Table 1. Simulation configurations

Mesh Resolution	**LISFLOOD**	**HEC RAS 1m sub-grid terrain resolution**	**HEC RAS 25/50/100m sub-grid terrain resolution**
25	L25	HR25_1	HR25_25
50	L50	HR50_1	HR50_50
100	L100	HR100_1	HR100_100

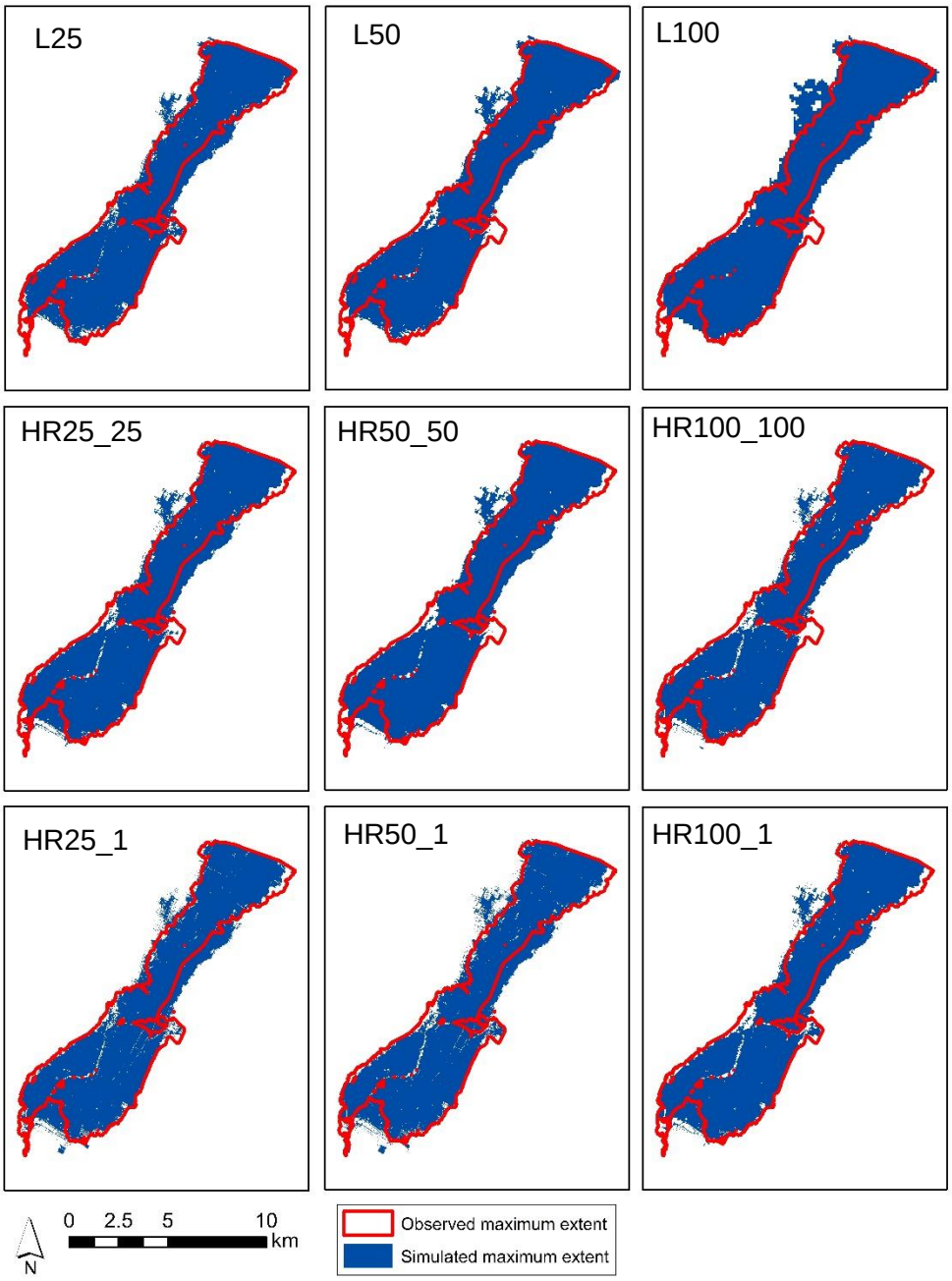

Figure 6. Overall simulated extent for all configurations (blue), compared to the observed extent (red outline)

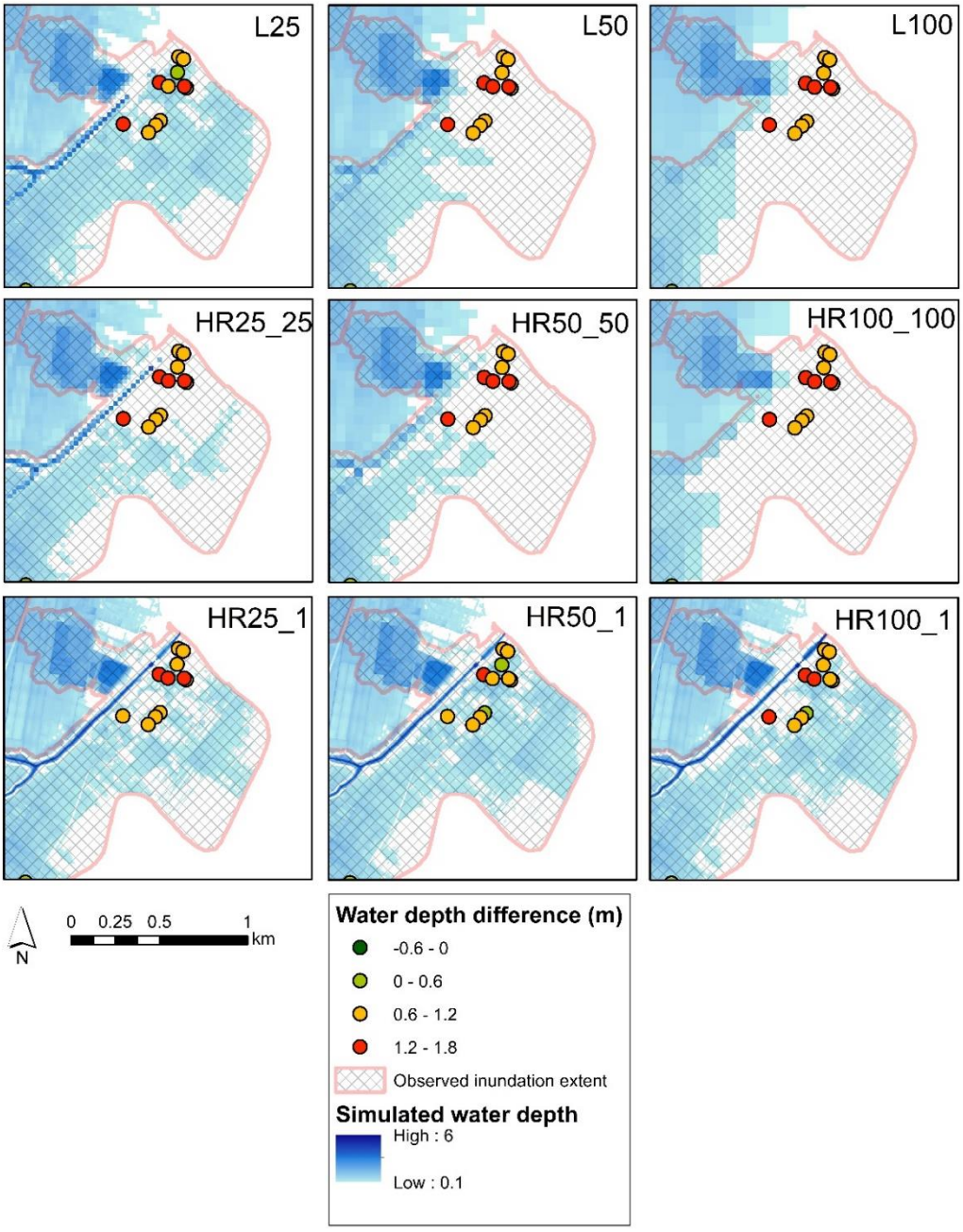

Figure 7. LISFLOOD-FP and HEC-RAS flood extent for different configurations at Bomporto (red box in Figure 5). Water depth difference (m) between predicted and observed at water mark points.

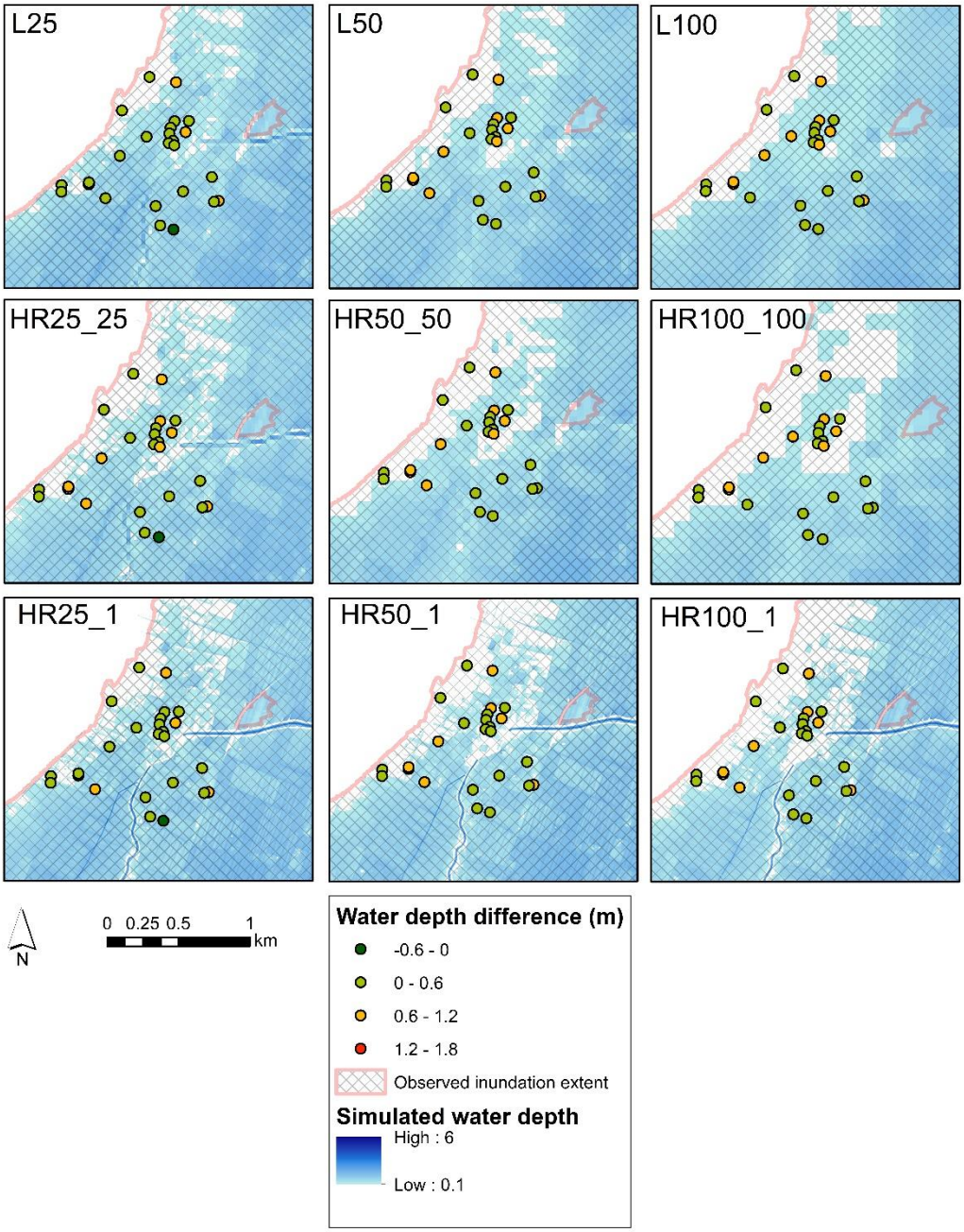

Figure 8. LISFLOOD-FP and HEC-RAS flood extent for different configurations at Bastiglia (green box in Figure 5). Water depth difference (m) between predicted and observed at water marks.

Table 2. Measure of Fit F (in %), inundation extent accuracy.

Mesh size[m]	LISFLOOD-FP	HEC-RAS 1m sub-grid	HEC-RAS 25/50/100m sub-grid
25	81	78	78
50	78	78	77
100	77	78	77

Table 3. RMSE [m] of the water depth at water marks

Mesh size [m]	LISFLOOD-FP	HEC-RAS 1m sub-grid	HEC-RAS 25/50/100m sub-grid
25	0.61	0.69	0.79
50	0.80	0.62	0.80
100	0.82	0.71	0.84

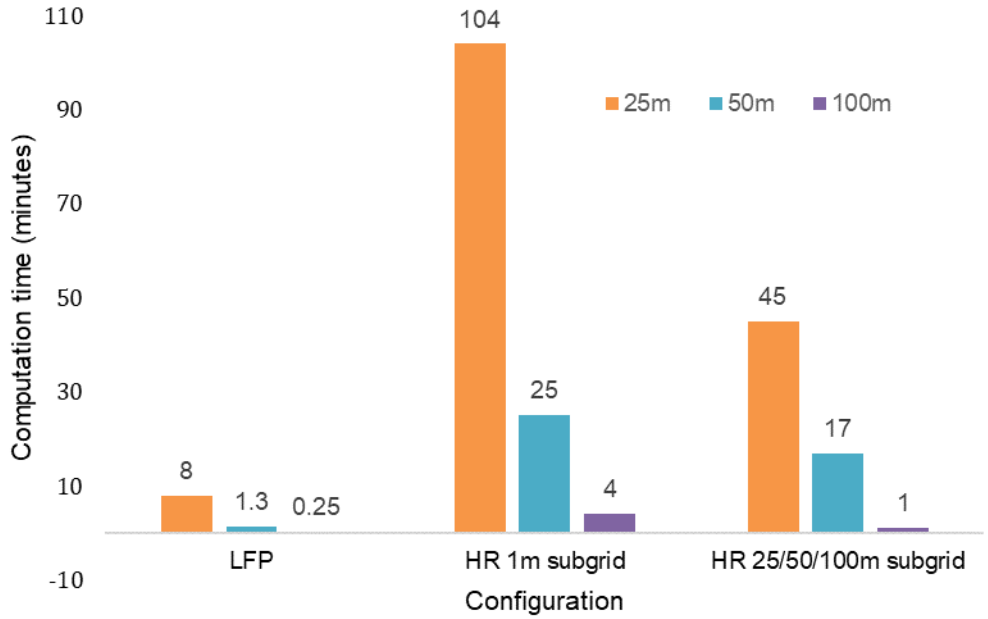

Figure 9. Approximate computation time of HEC-RAS and LISFLOOD-FP configurations

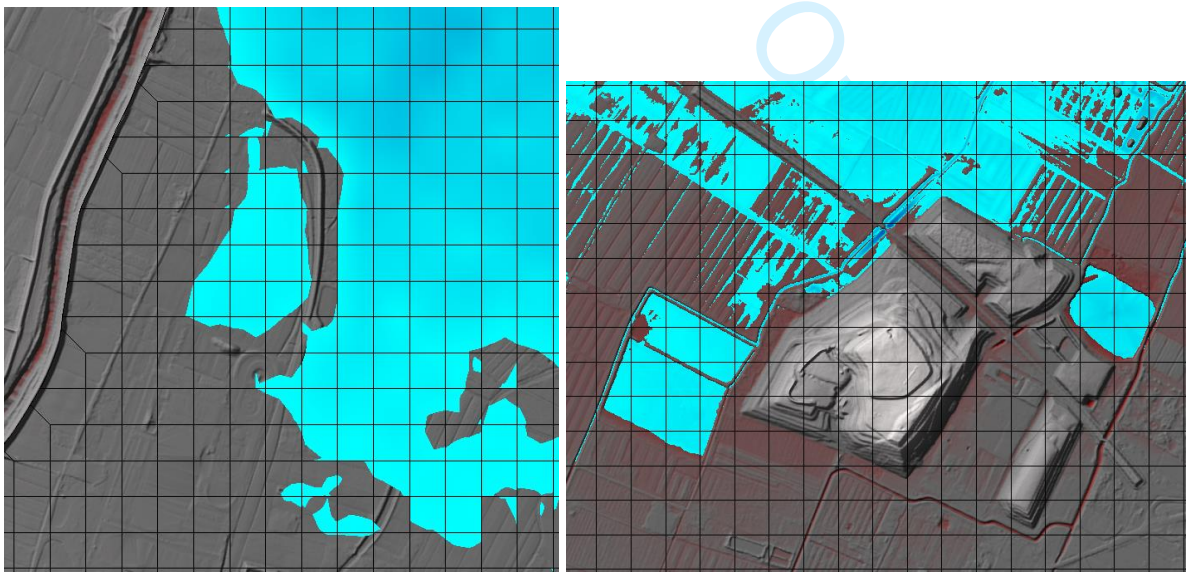

Figure 10. Leakage effect of HEC-RAS sub-grid mesh examples of HR100_100 (left), HR25_1 (right). Larger ponds of water in both images are disconnected from the inundation extent.

Figure 11. 25m resolution DEM. Dark blue - canal, light green – levee.